Available online at www.sciencedirect.com
ScienceDirect
Journal of Molecular Structure 826 (2007) 104–112
Journal of MOLECULAR STRUCTURE
www.elsevier.com/locate/molstruc

Syntheses, structures, photoluminescence and theoretical studies of two dimeric Zn(II) compounds with aromatic *N*,*O*-chelate phenolic ligands

Yi-Ping Tong [a,b], Shao-Liang Zheng [a,*], Xiao-Ming Chen [a,*]

[a] *State Key Laboratory of Optoelectronic Materials and Technologies/BISC Lab, School of Chemistry and Chemical Engineering, Sun Yat-Sen University, Guangzhou 510275, China*
[b] *Department of Chemistry, Hanshan Normal College, Chaozhou 521041, China*

Received 20 February 2006; accepted 20 April 2006
Available online 27 June 2006

Abstract

Two neutral and dimeric Zn(II) complexes $[Zn_2(epbm)_4]$ (**1**) and $[Zn_2(bpbm)_4]$ (**2**) (Hepbm = 3-ethyl-2-(2-hydroxyphenyl)-3*H*-benzimidazole, Hbpbm = 3-*n*-butyl-2-(2-hydroxyphenyl)-3*H*-benzimidazole) have been prepared and characterized by X-ray crystallography and photoluminescent studies. Time-dependent density functional theory (TDDFT) energy level calculation and molecular orbital calculation show their absorption and luminescence properties are ligand-centered. The spectral shifts caused by the effects of deprotonation/complextion, and substitution/dimerization have been also discussed. Both **1** and **2** show blue emission nature.

Keywords: Zn(II) complexes; Photoluminescence; Alkylation; Time-dependent density functional theory (TDDFT); Oligomerization; Benzimidazole derivatives

1. Introduction

As a basic component of full-color display in organic light-emission diodes (OLEDs), neutral and blue emission materials are required to be thermally stable [1]. Among a number of metal complexes found with excellent light emitting property in recent years [2,3], Zn(II) complexes with phenolic *N*,*O*-donor ligands showed application potential as blue or blue-green emitters in electroluminescence [4], as exemplified by monomeric $[Zn(pbm)_2]$ and $[Zn(apbm)_2]$ (Hpbm = 2-(2-hydroxyphenyl)-benzimidazole; and Hapbm = 5-amino-2-(1*H*-benzoimidazol-2-yl)phenol) [5], dimeric $[Zn_2(btz)_4]$ (Hbtz = 2-(2-hydroxyphenyl)-benzothiazole) [6], trimeric $[Zn_3(ppo)_6]$ (Hppo = 2-(2-hydroxyphenyl)-5-phenyl-1,3-oxazole) [7], and tetrameric $[Zn_4(q)_8]$ (Hq = 8-hydroxyquinoline) [8].

Phenolic *N*,*O*-donor derivatives can be used to construct neutral Zn(II) complexes with the structures ranging from monomers to oligomers or polymers (Scheme 1) [5–8]. With the *O*-donor atoms of deprotonated phenolate rings functioning as either terminal or bridging atoms, such ligands show a variety of coordination modes in ligating metal ions. Zn(II) ions may have different coordination numbers (commonly 4–6) in ligation to such phenolic *N*,*O*-donor derivatives in a variety of coordination geometries, which can be expected to have high luminescence in the blue or blue-green region [5–8]. An increase of the dihedral angle between the imidazole and phenolic rings, concomitant with an increase of the *N*- and *O*-donor separation, will usually enhance the probability of a bridging coordination mode, leading to polymerization of the resulting metal complexes.

We recently reported the synthesis, crystal structures, photoluminescence and theoretical calculations of a series of neutral and blue-luminescent mononuclear Be(II) and Zn(II) complexes, namely $[Be(pbm)_2]$, $[Be(pbx)_2]$, $[Be(pbt)_2]$ (Hpbx = 2-(2-hydroxylphenyl)benzoxazole, and Hpbt = 2-(2-hydroxyl-phenyl)benzothiazole) [9], $[Zn(pbm)_2]$ and $[Zn(apbm)_2]$ [5]. We anticipated that an alkylation

* Corresponding authors.
E-mail address: cxm@mail.sysu.edu.cn (X.-M. Chen).

0022-2860/$ - see front matter © 2006 Elsevier B.V. All rights reserved.
doi:10.1016/j.molstruc.2006.04.037

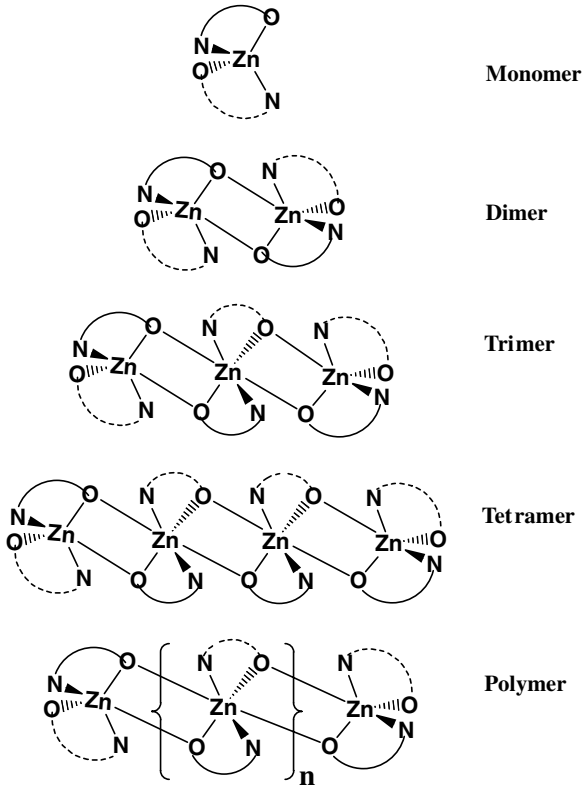

Scheme 1. Coordination modes of Zn(II) complexes with *N*,*O*-donor phenolic ligands.

modification of Hpbm at the imidazole-*N* position with steric hindrance can result in a markedly larger separation between *N*- and *O*-donor atoms and hence lead to the formation of new neutral and polymeric Zn(II) complexes. Indeed, we have synthesized two alkylated derivatives, namely 3-ethyl-2-(2-hydroxyphenyl)-3*H*-benzimidazole hydrochloride (Hepbm·HCl) and 3-*n*-butyl-2-(2-hydroxyphenyl)-3*H*-benzimidazole hydrochloride (Hbpbm·HCl·H_2O), which led to the generations of two new dimeric Zn(II) complexes $[Zn_2(epbm)_4]$ (**1**) and $[Zn_2(bpbm)_4]$ (**2**). Herein we report the synthesis, crystal structures, photoluminescence and time-dependent density functional theory (TDDFT) studies of these compounds.

2. Experimental

All the reagents and solvents employed were commercially available and used as received without further purification. The C, H and N micro-analyses were carried out with an Elementar Vario El elemental analyzer. The ^{1}H NMR data were recorded with a Varian INOVA500NB spectrometer. The FTIR spectra were recorded using a Bruker Vector22 spectrometer in the KBr pellets in the range 4000–400 cm^{-1}. The UV–vis spectra were recorded by a Varian Cary-100 spectrometer. The ESI-MS was carried out on a high-resolution Finnigan MAT LCQ mass spectrometer. The steady-state fluorescence lifetimes were determined with an Edinburgh Instrument FLS920 fluorescence spectrophotometer using laser light resource.

2.1. Preparation of Hepbm·HCl

Hpbm was synthesized using similar methods based on the literature [5,10]. Hepbm·HCl was synthesized from Hpbm based on a modified literature method [11]. Hpbm (0.210 g, 1 mmol) in acetone (100 mL) was added with KOH (0.169 g, 3 mmol) and then heated to reflux temperature. The mixture further reacted with excessive bromoethane (0.327 g, 3 mmol) by slow addition in small portions in ca. 1 h, and the reaction was maintained at the reflux condition for ca. 3 h before it was allowed to cool to room temperature, filtered off and washed with acetone. The combined filtrate was evaporated under reduced pressure to give a brown viscous oil. The crude material from the above reaction was then dissolved into pyridine (1 mL), and concentrated hydrochloric acid (1.2 mL) was added carefully with cooling in ice water. The water was distilled out of the mixture over a period of 1 h, and the reflux temperature of pyridinium hydrochloride (ca. 493 K) was then attained. The reaction was maintained for 1 h at this temperature before allowed to cool to ca. 373 K and then poured into cold water (ca. 10 mL) with stirring. The crude product was decolored with charcoal and filtered off and evaporated to dryness. After recrystallization, colorless crystals of Hepbm·HCl were isolated. The yield was ca. 70% calculated based on Hpbm. Calcd. for $C_{15}H_{15}Cl_1N_2O$: C, 65.57; H, 5.50; N, 10.20. Found: C, 65.39; H, 5.69; N, 10.05%; ^{1}H NMR (500 MHz, DMSO-d_6): δ 8.11 (m, 1H), 7.88 (m, 1H), 7.65 (m, 4H), 7.31 (d, $J = 8.10$ Hz, 1H), 7.10 (t, $J = 7.80$ Hz, 1H), 4.38 (q, $J = 7.50$ Hz, 2H), 1.36 (t, $J = 7.50$ Hz, 3H) ppm; FT-IR data (cm^{-1}): 3050s, 2794s, 2725s, 1608s, 1497m, 1461s, 1480m, 1352m, 1281m, 1262m, 1220m, 1160m, 1205w, 1117w, 1087w, 1057w, 831m, 756s, 686m, 588w, 538w, 421w.

2.2. Preparation of Hbpbm·HCl·H_2O

The synthetic approach was similar to that of Hepbm·HCl using 1-bromo-butane in place of bromoethane. The yield was ca. 70%. Calcd. For $C_{17}H_{21}Cl_1N_2O_2$: C, 63.65; H, 6.60; N, 8.73. Found: C, 63.71; H, 6.48; N, 8.79%; ^{1}H NMR (500 MHz, DMSO-d_6): δ 11.22 (s, 1H), 8.09 (m, 1H), 7.87 (m, 1H), 7.63 (m, 4H), 7.23 (d, $J = 7.80$ Hz, 1H), 7.10 (t, $J = 7.80$ Hz, 1H), 4.37 (t, $J = 7.20$ Hz, 2H), 1.70 (m, $J = 7.20$ Hz, 2H), 1.14 (m, $J = 7.20$ Hz, 2H), 0.71 (t, $J = 6.60$ Hz, 3H) ppm; FT-IR data (cm^{-1}): 3384m, 2961s, 1610s, 1594m, 1556m, 1499s, 1477m, 1463s, 1434m, 1357m, 1298m, 1325m, 1298m, 1212m, 1175m, 1159m, 1111m, 753s, 683w, 591w, 541w, 525m.

2.3. Preparation of $[Zn_2(epbm)_4]$ (**1**)

To a solution of zinc acetate dihydrate (0.110 g, 0.5 mmol) and Hepbm·HCl (0.275 g, 1.0 mmol) in ethanol (50 mL) was added a small amount of triethylamine and acetic acid to control the solution pH to ca. 6.0, the resultant solution was allowed to stand for very slow evaporation for

over 1 year at ambient temperature, colorless block crystals of **1** were obtained (yield ca. 0.108 g, 40%). ESI-MS (CH_2Cl_2): $m/z = 1080.8$ $[Zn_2L_4 + H]^+$. Calcd. for $C_{60}H_{52}N_8O_4Zn_2$: C, 66.73; H, 4.85; N, 10.38. Found: C, 66.63; H, 5.08; N, 10.25%; ^{1}H NMR (500 MHz, DMSO-d_6): δ 7.67 (d, $J = 5.40$ Hz, 8H), 7.44 (d, $J = 6.90$ Hz, 4H), 7.29 (t, $J = 7.20$ Hz, 12H), 6.94 (s, 8H), 4.27 (q, $J = 7.60$ Hz, 8H), 1.33 (t, $J = 7.60$ Hz, 12H) ppm; FT-IR data (cm^{-1}): 1596s, 1543m, 1504m, 1475s, 1428s, 1403m, 1309m, 1319m, 1261m, 1153m, 1133m, 1033m, 1011w, 865m, 748s, 736s, 704w, 574w, 547w, 480w.

2.4. Preparation of $[Zn_2(bpbm)_4]$ (**2**)

To an ethanol solution (50 mL) of zinc acetate dihydrate (0.110 g, 0.5 mmol) and Hbpbm·HCl·H_2O (0.320 g, 1.0 mmol) was added a small amount of triethylamine and acetic acid to control the solution PH to ca. 6.0, the resultant solution was allowed to stand for very slow evaporation for over 14 months at ambient temperature, colorless block crystals of **2** were obtained (yield ca. 0.122 g, 41%). ESI-MS (CH_2Cl_2): $m/z = 1193.1$ $[Zn_2L_4 + H]^+$. Calcd. for $C_{68}H_{68}N_8O_4Zn_2$: C, 68.51; H, 5.75; N, 9.40. Found: C, 68.29; H, 5.55; N, 9.39%; ^{1}H NMR (500 MHz, DMSO-d_6): δ 7.67 (d, $J = 5.40$ Hz, 8H), 7.46 (d, $J = 6.90$ Hz, 4H), 7.28 (m, 12H), 6.91 (m, 8H), 4.32 (t, $J = 7.30$ Hz, 8H), 1.72 (m, 8H), 1.17 (m, 8H), 0.77 (t, $J = 6.70$ Hz, 12H) ppm; FT-IR (cm^{-1}): 1601m, 1560w, 1496s, 1501m, 1428m, 1406m, 1340m, 1309w, 1265m, 1219w, 1151w, 1125w, 1032w, 1011w, 861w, 751m, 743m, 575w.

2.5. X-ray crystallography

Diffraction intensities for **1**, **2**, Hepbm·HCl and Hbpbm·HCl·H_2O were collected at 293 K or 123 K on a Bruker Smart Apex CCD diffractometer (Mo$K\alpha$, $\lambda = 0.71073$ Å′). Absorption corrections were applied by using SADABS [12]. The structures were solved with direct methods and refined with full-matrix least-squares technique using SHELXTL program package [13]. The organic hydrogen atoms were generated in ideal positions and the aqua hydrogen atoms were located from difference maps. Anisotropic thermal parameters were applied to all non-hydrogen atoms. Experimental details of the X-ray analyses are provided in Table 1. Selected bond lengths and angles are listed in Table 2.

2.6. Calculation details

Based on the optimized geometries (with no constraints during the optimizations), time-dependent density functional (TDDFT) calculations and molecular orbital calculations were performed at the B3LYP level with 6-31G** basis set for C, H, N and O atoms, and effective core potentials basis set LanL2DZ for Zn atoms, employing the Gaussian98 suite of programs [14]. The electron density diagrams of molecular orbitals were obtained with the Molden 3.5 graphics program [15].

3. Results and discussion

3.1. Synthesis and stability

Ethyl and *n*-butyl groups were selected as substituent groups to modify Hpbm, which led to successful controlling the formations of new dimeric Zn(II) complexes different from the neutral, monomeric complex $[Zn(pbm)_2]$. The synthetic routines for Hpbm and its *N*-ethyl or *N*-*n*-butyl substituted derivatives (Hepbm·HCl and Hbpbm·HCl·H_2O) are shown in Scheme 2.

Table 1
Crystal data and structure refinement for **1**, **2**, Hepbm·HCl and Hbpbm·HCl·H_2O

Compound	Hepbm·HCl	Hbpbm·HCl·H_2O	**1**	**2**
Formula	$C_{15}H_{15}ClN_2O$	$C_{17}H_{21}ClN_2O_2$	$C_{60}H_{52}N_8O_4Zn_2$	$C_{68}H_{68}N_8O_4Zn_2$
Formula mass	274.74	320.81	1079.84	1192.04
Crystal system	Triclinic	Monoclinic	Monoclinic	Triclinic
Space group	*P*-1 (No. 2)	$P2_1/c$ (No. 14)	$P2_1/c$ (No. 14)	*P*-1 (No. 2)
a/Å	8.3349(8)	9.2883(8)	10.528(2)	10.912(1)
b/Å	9.2688(8)	19.8996(18)	21.150(4)	11.0509(11)
c/Å	9.7149(9)	9.5452(9)	14.398(2)	13.5192(13)
α/°	94.259(2)	90	90	75.749(2)
β/°	113.091(1)	103.858(2)	130.257(9)	86.102(2)
γ/°	91.377(2)	90	90	64.946(2)
V/Å^3	687.33(11)	1712.9(3)	2446.6(7)	1430.2(2)
Z	2	4	2	1
D_c/g cm^{-3}	1.328	1.244	1.466	1.384
μ/mm^{-1}	0.271	0.231	1.041	0.897
Unique refl.	1973	3362	4788	5842
S on F^2	1.048	1.078	0.981	1.084
R_1 [$I > 2\sigma(I)$]	0.0355	0.0679	0.0669	0.0476
wR_2 [$I > 2\sigma(I)$]	0.0912	0.1734	0.1250	0.1196
R_1 (all data)	0.0396	0.0848	0.1379	0.0602
wR_2 (all data)	0.0945	0.1858	0.1517	0.1311

Table 2
Selected bond length (Å) and angles (°) for **1**, **2**, Hepbm·HCl and Hbpbm·HCl·H_2O

1			
Zn(1)–O(2a)	1.973(3)	Zn(1)–N(3)	2.042(4)
Zn(1)–N(1)	2.032(4)	Zn(1)–O(2)	2.210(3)
Zn(1)–O(1)	2.035(3)		
O(2a)–Zn(1)–N(1)	117.7(2)	O(1)–Zn(1)–N(3)	96.9(2)
O(2a)–Zn(1)–O(1)	104.1(2)	O(2a)–Zn(1)–O(2)	73.7(1)
N(1)–Zn(1)–O(1)	87.2(2)	N(1)–Zn(1)–O(2)	96.8(2)
O(2a)–Zn(1)–N(3)	119.4(2)	O(1)–Zn(1)–O(2)	175.9(1)
N(1)–Zn(1)–N(3)	119.6(2)	N(3)–Zn(1)–O(2)	81.5(2)
Zn(1a)–O(2)–Zn(1)	106.3(1)		
2			
Zn(1)–O(2a)	1.980(2)	Zn(1)–N(1)	2.046(2)
Zn(1)–O(1)	2.020(2)	Zn(1)–O(2)	2.186(2)
Zn(1)–N(3)	2.043(2)		
O(2a)–Zn(1)–O(1)	97.76(8)	N(3)–Zn(1)–N(1)	119.67(9)
O(2a)–Zn(1)–N(3)	115.66(8)	O(2a)–Zn(1)–O(2)	74.27(8)
O(1)–Zn(1)–N(3)	99.32(8)	O(1)–Zn(1)–O(2)	171.98(7)
O(2a)–Zn(1)–N(1)	122.38(8)	N(3)–Zn(1)–O(2)	83.69(8)
O(1)–Zn(1)–N(1)	88.37(8)	N(1)–Zn(1)–O(2)	96.63(8)
Zn(1a)–O(2)–Zn(1)	105.73(8)		
Hepbm·HCl			
O(1)–C(1)	1.351(3)	N(2)–C(8)	1.400(2)
N(1)–C(7)	1.336(2)	N(2)–C(14)	1.471(3)
N(1)–C(13)	1.383(3)	C(6)–C(7)	1.462(3)
N(2)–C(7)	1.337(2)		
C(7)–N(1)–C(13)	109.3(2)	N(1)–C(7)–N(2)	109.2(2)
C(7)–N(2)–C(8)	108.2(2)	N(1)–C(7)–C(6)	122.2(2)
C(7)–N(2)–C(14)	126.7(2)	N(2)–C(7)–C(6)	128.5(2)
C(8)–N(2)–C(14)	124.9(2)	C(8)–C(13)–N(1)	106.5(2)
Hbpbm·HCl·H_2O			
N(2)–C(7)	1.343(4)	N(1)–C(7)	1.332(4)
N(2)–C(8)	1.397(4)	N(1)–C(13)	1.379(4)
N(2)–C(14)	1.462(4)	C(7)–C(6)	1.467(4)
O(1)–C(1)	1.356(3)		
C(7)–N(2)–C(8)	108.0(2)	N(1)–C(7)–N(2)	109.0(2)
C(7)–N(2)–C(14)	126.9(2)	N(1)–C(7)–C(6)	123.1(3)
C(8)–N(2)–C(14)	125.0(2)	N(2)–C(7)–C(6)	127.6(3)
C(7)–N(1)–C(13)	109.7(3)	C(13)–C(8)–N(2)	107.0(2)

Symmetric codes: **1**: $a = -x+1, -y, -z+1$; **2**: $a = -x, -y+1, -z+2$.

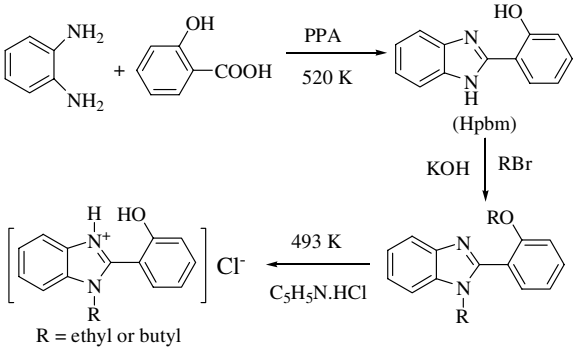

Scheme 2. The synthetic routes for Hepbm·HCl (R = ethyl) and Hbpbm·HCl·H_2O (R = butyl).

Similar to other related neutral complexes [5,9], the single crystals of **1** and **2** were very hard to grow. Although different techniques were employed to grow the single crystals of X-ray quality, including conventional evaporation, diffusion and solvo(hydro)thermal methods, the single crystals were only successfully isolated by conventional evaporation after 1 year, hence we can have a systematic investigation of their emission properties using TDDFT calculations and/or molecular orbital calculations, avoiding dubious conclusions of the luminescent property arguments without the X-ray structures that are much more complicated than their empirical formulae.

Thermal stabilities of **1** and **2** were characterized by thermo-gravimetric analysis (TGA) under flowing N_2 gas at a heating rate of 10 °C/min. **2** had a much higher thermally stable temperature of 454 °C, while **1** was thermally unstable above 267 °C, where **1** likely experienced a de-ethyl process, as indicated by a weight loss of ca. 10.70%.

3.2. Crystal structures of the ligands

Single-crystal X-ray structure analysis indicated that Hpbm is a neutral and approximately planar molecule with the dihedral angle between benzimidazole and phenolic rings at ca. 2.2° [5], being similar to other planar phenolic *N,O*-donor ligands Hpbx and Hpbt. The distance between the *N*- and *O*-donor atoms is ca. 2.564 Å for Hpbm.

The organic species for crystalline Hepbm·HCl and Hbpbm·HCl·H_2O were characterized to be protonated in the solid (Fig. 1). Compared to the un-alkylated Hpbm, the *N*-ethyl or *N*-butyl group in $[H_2epbm]^+$ or $[H_2bpbm]^+$

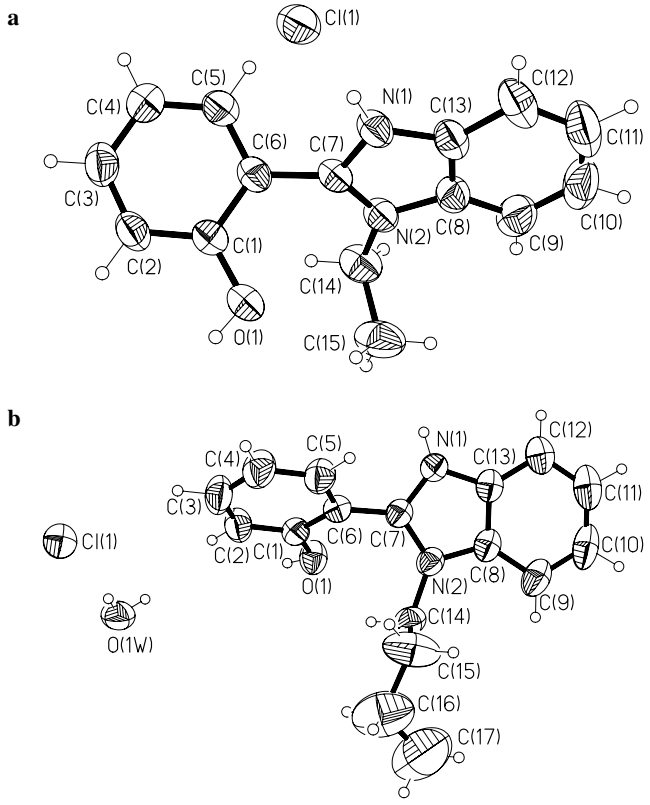

Fig. 1. Perspective views of Hepbm·HCl (a) and Hbpbm·HCl·H_2O (b). Thermal ellipsoids are plotted at the 50% probability level.

generates significantly steric hindrance, and hence larger dihedral angles of ca. 58.2° and 56.6° between the imidazole and phenolic rings, as well as much larger separations between the *N*- and *O*-donor atoms (ca. 3.852 Å for $[H_2epbm]^+$ and 3.892 Å for $[H_2bpbm]^+$).

In the crystal packing of Hepbm·HCl, each chloride ion accepts two hydrogen bonds from adjacent phenolic and imidazole groups [O(1A)···Cl(1) 3.078(2) Å; N(1)···Cl(1) 3.059(2) Å] of two $[H_2epbm]^+$ ions (Fig. 2(a)), while strong π–π stacking interactions (interplanar distance ca. 3.47 Å) between the phenolic rings of adjacent $[H_2epbm]^+$ cations are also observed. While in the molecular packing of Hbpbm·HCl·H_2O, each chloride ion accepts three hydrogen bonds from the phenolic group [O(1)···Cl(1A) 3.057(2) Å] and two lattice water molecules [O(1WA)···Cl(1A) 3.180(3) and O(1W)···Cl(1A) 3.164(3) Å, (see Fig. 2(b))]; a strong hydrogen bond between the imidazole group and a lattice water molecule [N···O 2.693(4) Å] is also found.

3.3. Crystal Structures of **1** and **2**

Both **1** and **2** have similar centrosymmetrical Zn_2O_2 dimer structures (Fig. 3), which are planar and similar to those Zn_2O_2 cores documented previously [6]. Each Zn_2O_2 core is surrounded by four deprotonated $epbm^-$ or $bpbm^-$ ligands. A pair of these ligands act in the bridging mode and the other pair of ligands act in the chelate mode as terminal ligands, furnishing in a trigonal-bipyramidal arrangement for each Zn(II) ion with N(1), N(3) and O(2A) atoms at the equatorial positions, O(1) and O(2) atoms at the axial positions. The dihedral angles between benzimidazole and phenolate rings are 39.7° and 41.5° for **1**, and 40.9° and 43.9° for **2**, indicating non-coplanar nature.

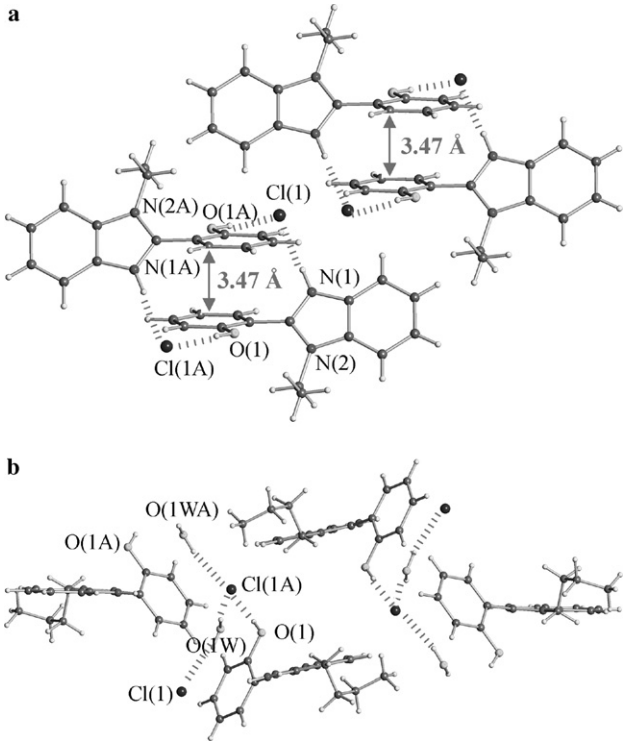

Fig. 2. Perspective views of hydrogen-bonding and π–π interactions for Hepbm·HCl (a) and Hbpbm·HCl·H_2O (b). Symmetry code for Hepbm·HCl: A: $1-x, 1-y, 1-z$; Hbpbm·HCl·H_2O: A: $x, 1/2-y, -1/2+z$.

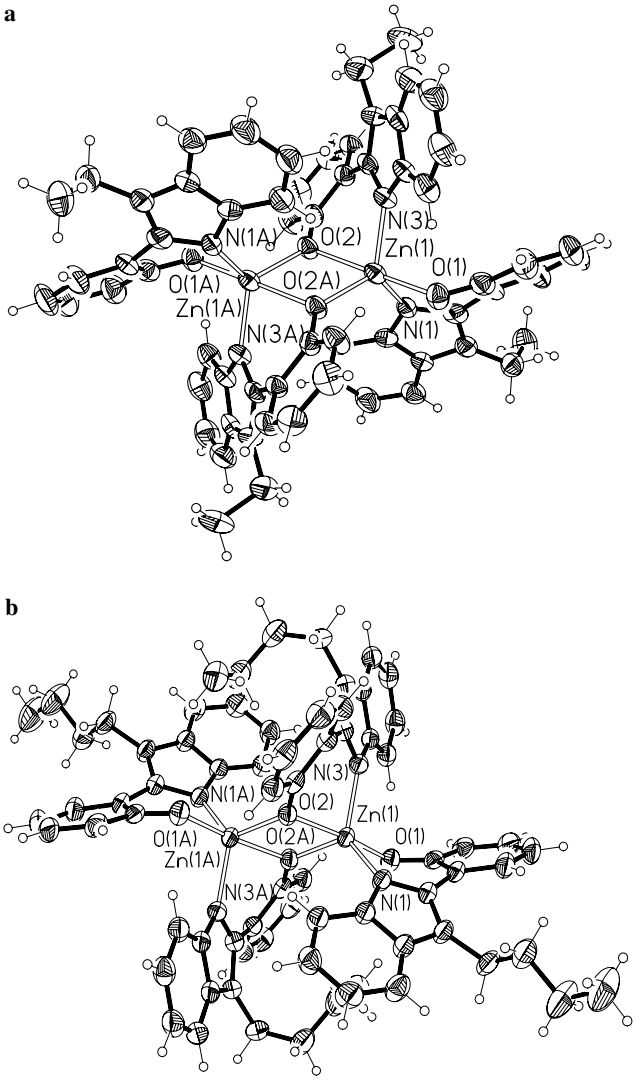

Fig. 3. Perspective view of **1** (a) and **2** (b) with the thermal ellipsoids at 50% probability level. Symmetry code for **1**: A: $1-x, -y, 1-z$; **2**: A: $-x, 1-y, 2-z$.

The hydrogen bonding and π–π stacking interactions are obviously weaker in both **1** and **2**, compared with the un-alkylated compound $[Zn(pbm)_2]$ [5]. This fact can be readily attributed to the presence of bulky alkyl groups that can reduce intermolecular π–π stacking interactions, while alkylation of the imidazole group can also reduce the formation of strong hydrogen bonds between benzimidazole donor and other acceptor atoms.

3.4. UV–vis and luminescent spectra

The lowest-energy absorption bands of Hepbm·HCl and Hbpbm·HCl·H_2O occur at 281 and 282 nm for the

Table 3
Calculated and experimental absorption wavelengths (nm) and transition nature for **1**, **2**, Hepbm·HCl and Hbpbm·HCl·H_2O with oscillator strengths in CH_2CI_2 and solid

Compound	Transition Nature	Wavelength			Oscillator strengths
		Exp. in CH_2Cl_2[b]	Exp. in solid	Calcd.	
Hepbm·HCl	$\pi \rightarrow \pi^*$	280	281	301	0.15
Hbpbm·HCl·H_2O	$\pi \rightarrow \pi^*$	281	282	302	0.16
Hpbm[a] (non-alkylated product)	$\pi \rightarrow \pi^*$	323	342	313	0.44
1	$\pi \rightarrow \pi^*$	322	343	351	0.14
2	$\pi \rightarrow \pi^*$	330	345	353	0.15
$[Zn(pbm)_2]$[a] (non-alkylated product)	$\pi \rightarrow \pi^*$	331	377	364	0.24

[a] The calculated and experimental results were reported in Ref. [5].
[b] The solution concentration is ca. 10^{-6} M.

powdered solid samples, and 280 and 281 nm in dichloromethane (ca. 10^{-6} M), respectively, while those of **1** and **2** lie in the visible region (343 and 345 nm for solid samples, and 322 and 330 nm for dichloromethane solutions (ca. 10^{-6} M), respectively) (Table 3, Fig 4). In general, the lowest-energy absorption bands may be attributed to the transitions from the ground-states to the higher-energy excited-states in UV spectra [16]. According to our TDDFT calculations, the lowest energy absorption maxima for $[H_2epbm]^+$ and $[H_2bpbm]^+$ cations (301 and 302 nm, respectively), which are consistent with those of experimental results, mainly arise from the transitions from the ground state to the first singlet excited state (S_0–S_1, with corresponding oscillator strengths 0.15 and 0.16, respectively) (Fig. 5(a)). The close approach of the calculated lowest energy absorption bands between them implies that the substitutions of ethyl and *n*-butyl group have an approximately identical effect on the absorption spectra, in accordance with the experimental results. However, the lowest energy absorption maxima for **1** and **2** are markedly red-shifted in the spectra, when compared to their ligands. Based on our TDDFT calculations, the corresponding lowest energy absorptions (351 and 353 nm, respectively) arise mainly from the transition from S_0–S_6 with oscillator strengths of 0.14 and 0.15 for **1** and **2** (Fig. 5(b)), respectively, while the transitions from S_0–S_1 (further into visible region of 371 and 372 nm, respectively) are relatively weaker (oscillator strength being 0.03). The calculated lowest energy absorption maxima (351 nm for **1** and 353 nm for **2**) are in good agreement with the experimental observations. The excited-state–ground-state (ES–GS) separations derived from TDDFT calculations are in agreement with those observed experimentally.

For the $[H_2epbm]^+$ and $[H_2bpbm]^+$ cations, the S_0–S_1 transitions are mainly associated with their HOMOs and LUMOs with configuration interaction coefficient up to 0.67; the HOMOs are π bonding orbitals and LUMOs are π^* anti-bonding orbitals (Fig. 6), thus the transitions should be ascribed to $\pi \rightarrow \pi^*$ transition in nature. However, the S_0–S_1 transitions are mainly associated with transitions

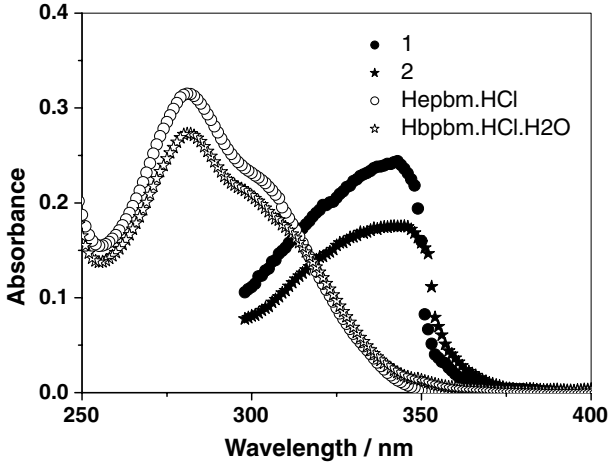

Fig. 4. The UV–vis spectra for Hepbm·HCl, Hbpbm·HCl·H_2O, **1** and **2** in solid state.

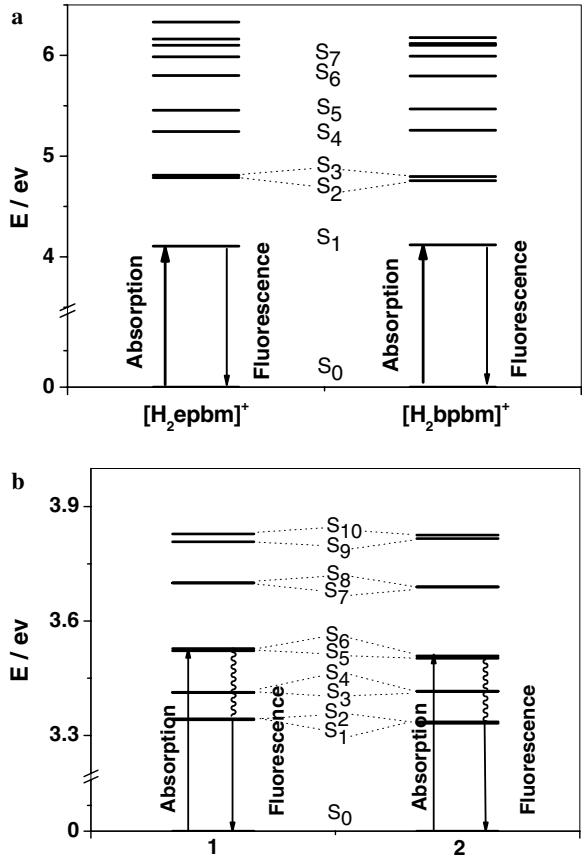

Fig. 5. The singlet excited state diagrams of ligands ($[H_2epbm]^+$ and $[H_2bpbm]^+$) (a) and complexes (**1** and **2**) (b).

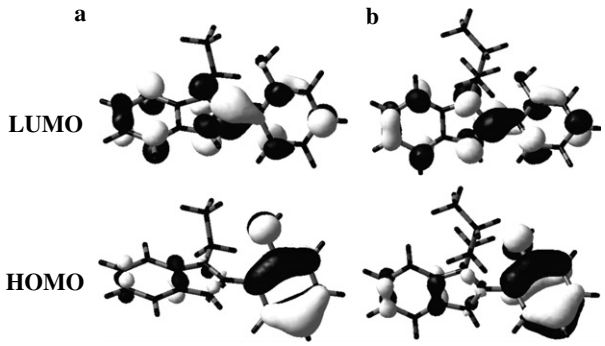

Fig. 6. Contour plots of HOMOs and LUMOs of the cations of $[H_2epbm]^+$ (a) and $[H_2bpbm]^+$ (b).

from HOMO − 1 to LUMO with configuration interaction coefficients up to 0.52 and 0.48 for **1** and **2**, respectively, and from HOMO to LUMO + 1 with the configuration interaction coefficients up to 0.47 and 0.51, respectively. The HOMO and HOMO − 1 orbitals are π bonding orbitals of the deprotonated ligands, and LUMO and LUMO + 1 orbitals are π^* anti-bonding orbitals of deprotonated ligands (Fig. 7), therefore the transitions should be also ascribed to $\pi \rightarrow \pi^*$ in nature and should be of ligand-centered charge transfer (LCCT).

For the S_0–S_6 transitions of **1** and **2**, the transition compositions are mainly HOMO − 1 → LUMO + 2 (coefficient up to 0.43) and HOMO → LUMO + 3 (coefficient up to 0.41) for **1** and HOMO − 1 → LUMO + 3 (coefficient up to 0.43) and HOMO → LUMO + 2 (coefficient up to 0.47) for **2**, although such transitions are also assigned to be $\pi \rightarrow \pi^*$ transition in nature in terms of our TDDFT results (Fig. 7). Similarly, they are ligand-centered charge transfer (LCCT).

It is notable that *n*-butyl is a slightly stronger electron-donor than ethyl group, thus **2** should be slightly smaller in energy gap than **1**, similarly, Hbpbm·HCl·H_2O is slightly smaller in energy gap with respect to Hepbm·HCl. These are in good agreement with the ES–GS separation of our TDDFT calculations and experimental UV spectra both in solid and in dichloromethane. However, compared with un-alkylated Hpbm and $[Zn(pbm)_2]$ (Table 3) [5], the alkylation twists the ligand into a non-planar structure, as indicated by the dihedral angle between benzimidazole and phenolic rings, resulting in the reduction of electron delocalization energy, thus an increase of energy gap can be assumed. Meanwhile, the reduction of energy gap for the alkylated products caused by the electron-donating *n*-butyl or ethyl group is much smaller, thus a significant overall increase of energy separation resulting from the alkylation and/or oligomerization can be expected, in good agreement with the fact that the S_0–S_1 energy separation of our TDDFT calculations and experimental absorption maxima both in solid and dichloromethane solution for the alkylated products are all larger in energy than those of their un-alkylated species. Moreover, the variations of supramolecular interactions caused by the alkylation and/or oligomerization (mentioned above) are also favoured for the blue-shifts of UV spectra in solid with respect to their un-alkylated parents [17,18].

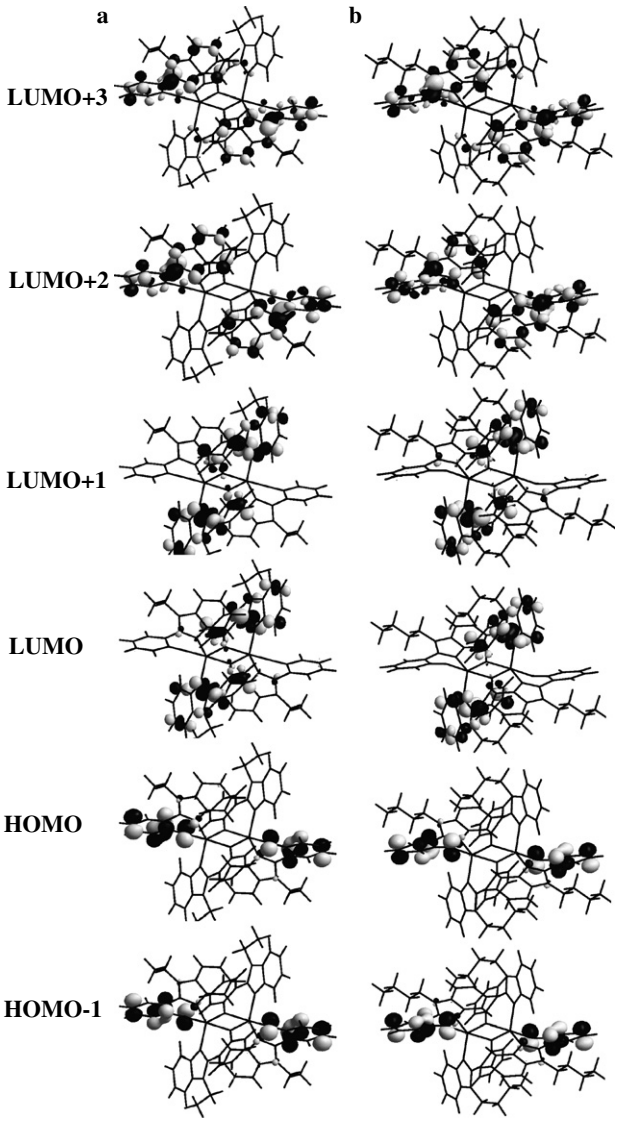

Fig. 7. Contour plots of relevant molecular orbitals (from HOMO − 1 to LUMO + 3) of **1** (a) and **2** (b).

Deprotonation and complexation of ligands with Zn(II) ions will usually reduce significantly the energy gaps between LUMOs and HOMOs [3,5,19] and therefore according to the energy-gap law for radiationless deactivation [20,21], leading to the reduction of emission energy. The emission maxima for Hepbm·HCl and Hbpbm·HCl·H_2O are 382 nm (λ_{ex} = 325 nm) and 388 nm (λ_{ex} = 330 nm), respectively (Fig. 8), while those for **1** and **2** are 422 nm (λ_{ex} = 367 nm) and 424 nm (λ_{ex} = 372 nm) in solid, respectively. According to our TDDFT calculations, the S_0–S_1 transitions for **1** and **2** are red-shifted when compared to their parent ligands, and this fact can also be readily related to the observations that **1** and **2** have smaller emission energy with respect to their parents. However, when compared with their un-alkylated species Hpbm and $[Zn(pbm)_2]$ [5], the emission energy is

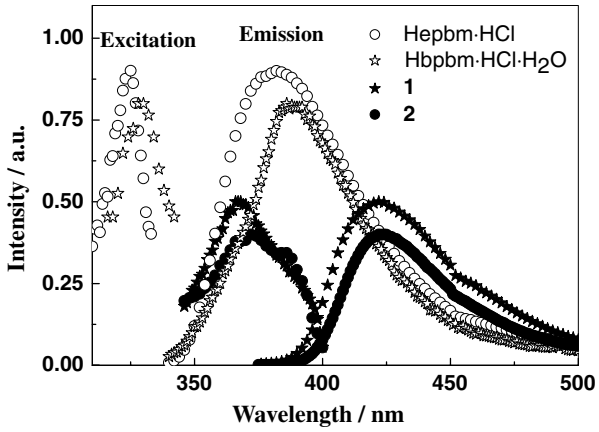

Fig. 8. The excitation and emission spectra for **1**, **2**, Hepbm·HCl and Hbpbm·HCl·H_2O in solid state.

significantly blue-shifted, respectively, which is in proper agreement with the ES–GS separations derived from our TDDFT calculations and experimental observations in UV spectra. Moreover, such blue-shifts of emission energy for the free ligands (up to 62 nm for Hepbm·HCl vs. Hpbm, and 56 nm for Hbpbm·HCl·H_2O vs. Hpbm) are much larger than their corresponding Zn(II) complexes (only 12 nm for **1** vs. [Zn(pbm)$_2$], and 10 nm for **2** vs. [Zn(pbm)$_2$]), in agreement with the fact that the excited-state intramolecular proton transfer (ESIPT) processes are present in crystalline unalkylated Hpbm [5,9,22], but absent in crystalline alkylated Hepbm·HCl and Hbpbm·HCl·H_2O.

The emission lifetimes for **1** and **2** in solid at 298 K were measured to be 1.92 and 2.34 ns, respectively, which are similar to those of other related Zn(II) complexes [3,5].

4. Conclusions

Two new neutral Zn(II) complexes with dimeric structures have been synthesized based on the alkylation modification of a phenolic *N*,*O*-donor derivative at the imidazole group of Hpbm, which twists the ligand and hence furnishes dimeric Zn(II) compounds emitting blue luminescence. The TDDFT level calculations demonstrate that their absorption and luminescent properties are all ligand-centered and $\pi \rightarrow \pi^*$ transitions in nature. Also interestingly, the *n*-butylated Zn(II) complex exhibited a much better thermal stability compared to the ethylated one, implying the better potential of *n*-butyl group in the preparations of luminescent films for OLED through vacuum deposition.

5. Supporting information available

Crystallographic data for the structural analysis have been deposited with the Cambridge Crystallographic Data Centre (Deposition Nos. CCDC-269149, 269150, 269153 and 269154 for Hepbm·HCl and Hbpbm·HCl·H_2O, **1** and **2**, respectively).

Acknowledgements

This work was supported by the National Natural Science Foundation of China (Grant No. 20531070) and a Scientific and Technological Project of Guangdong Province (No. 04205405).

References

[1] H.S. Nalwa, L.S. Rohwer, A.J. Heeger (Eds.), Handbook of Luminescence, Display Materials, and Devices, American Scientific Publishers, Stevenson Ranch, CA, 2003, and references cited therein.
[2] (a) S.-F. Liu, Q. Wu, H.L. Schmider, H. Aziz, N.-X. Hu, Z. Popović, S. Wang, J. Am. Chem. Soc. 122 (2000) 3671;
(b) Y. Cui, Q.-D. Liu, D.-R. Bai, W.-L. Jia, Y. Tao, S. Wang, Inorg. Chem. 44 (2005) 601;
(c) S. Wang, Coord. Chem. Rev. 215 (2001) 79.
[3] (a) S.-L. Zheng, J.-H. Yang, X.-L. Yu, X.-M. Chen, W.-T. Wong, Inorg. Chem. 43 (2004) 830;
(b) S.-L. Zheng, J.-P. Zhang, X.-M. Chen, Z.-L. Huang, Z.-Y. Lin, W.-T. Wong, Eur. J. Chem. 9 (2003) 3888;
(c) S.-L. Zheng, X.-M. Chen, Aust. J. Chem. 57 (2004) 703.
[4] (a) Y. Hamada, T. Sano, H. Fujii, Y. Nishio, H. Takahashi, K. Shibata, Jpn. J. Appl. Phys. 35 (1996) L1339;
(b) N. Nakamura, S. Wakabayashi, K. Miyairi, T. Fujii, Chem. Lett. (1994) 1741.
[5] Y.-P. Tong, S.-L. Zheng, X.-M. Chen, Eur. J. Inorg. Chem. (2005) 3734.
[6] G. Yu, S. Yin, Y. Liu, Z. Shuai, D. Zhu, J. Am. Chem. Soc. 125 (2003) 14816.
[7] T.S. Kim, T. Okubo, T. Mitani, Chem. Mater. 15 (2003) 4949.
[8] L.S. Sapochak, F.E. Benincasa, R.S. Schofield, J.L. Baker, K.K.C. Riccio, D. Fogarty, H. Kohlmann, K.F. Ferris, P.E. Burrows, J. Am. Chem. Soc. 124 (2002) 6119.
[9] Y.-P. Tong, S.-L. Zheng, X.-M. Chen, Inorg. Chem. 44 (2005) 4270.
[10] A.W. Addison, P.J. Burke, J. Heterocyclic Chem. 18 (1981) 803.
[11] D.J. Crane, E. Sinn, B. Tann, Polyhedron 18 (1999) 1527.
[12] R. Blessing, Acta Crystallogr. A 51 (1995) 33.
[13] G.M. Sheldrick, SHELXTL 6.10, Bruker Analytical Instrumentation, Madison, Wisconsin, USA, 2000.
[14] M.J. Frisch, G.W. Trucks, H.B. Schlegel, G.E. Scuseria, M.A. Robb, J.R. Cheeseman, V.G. Zakrzewski, J.A. Montgomery, R.E. Stratmann, J.C. Burant, S. Dapprich, J.M. Millam, A.D. Daniels, K.N. Kudin, M.C. Strain, O. Farkas, J. Tomasi, V. Barone, M. Cossi, R. Cammi, B. Mennuci, C. Pomelli, C. Adamo, S. Clifford, J. Ochterski, G.A. Petersson, P.Y. Ayala, Q. Cui, K. Morokuma, D.K. Malick, A.D. Rabuck, K. Raghavachari, J.B. Foresman, J. Cioslowski, J.V. Oritz, B.B. Stefanov, G. Liu, A. Liashenko, P. Piskorz, I. Komaromi, R. Gomperts, R.L. Martin, D.J. Fox, T. Keith, M.A. Al-Laham, C.Y. Peng, A. Nanayakkara, C. Gonzalez, M. Challacombe, P.M.W. Gill, B.G. Johnson, W. Chen, M.W. Wong, J.L. Andres, M. Head-Gordon, E.S. Replogle, J.A. Pople, GAUSSIAN 98, Revision A9; Gaussian, Inc., Pittsburgh, PA, 1998.
[15] G. Schaftenaar, Molden, Version 3.5, CAOS/CAMM Center Nijmegen, Toernooiveld, Nijmegen, The Netherlands, 1999.
[16] (a) N.J. Turro, K.-C. Liu, M.-F. Show, P. Lee, Photochem. Photobiol. 27 (1978) 523;
(b) S.-L. Zheng, P. Coppens, Cryst. Eng. Comm. 7 (2005) 289;
(c) S.-L. Zheng, P. Coppens, Chem. Eur. J. 11 (2005) 3583;
(d) S.-L. Zheng, P. Coppens, Cryst. Growth Des. 5 (2005) 2050.
[17] (a) P. Cassoux, Science 291 (2001) 263;
(b) H. Tanaka, Y. Okano, H. Kobayashi, W. Suzuki, A. Kobayashi, Science 291 (2001) 285;
(c) A. Kobayashi, H. Tanaka, H. Kobayashi, J. Mater. Chem. 11 (2001) 2078.
[18] B. Valeur, Molecular Fluorescence: Principles and Applications, Wiley-VCH, Weinheim, 2002.

[19] V.W.-W. Yam, Y.-L. Pui, K.-K. Cheung, Inorg. Chem. 39 (2000) 5741.
[20] (a) N.J. Turro, Modern Molecular Photochemistry, University Science Books, Sausalito, CA, 1991;
(b) J.M. Klessinger, J. Michl, Excited States and Photochemistry of Organic Molecules, VCH, New York, 1995, and references cited therein.
[21] D.V. Scaltrito, D.W. Thompson, J.A. O'Callaghan, G.J. Meyer, Coord. Chem. Rev. 208 (2000) 243, and references cited therein.
[22] J. Waluk, Conformational Analysis of Molecules in Excited States, Wiley-VCH, Weinheim, 2000, and references cited therein, pp. 83–85.